DOI: 10.1002/ejic.201100213

In Situ Tetrazole Ligand Synthesis of Two-Fold Interpenetrating Zinc Coordination Frameworks

Li Ma,[a] Yong-Cai Qiu,[a] Guo Peng,[a] Jin-Biao Cai,[a] and Hong Deng*[a]

Keywords: N ligands / Metal organic frameworks / Interpenetrating networks / Zinc / Luminescence

Four d^{10} metal directed coordination frameworks, $[Zn_2(MT)_3(IN)]$ (**1**; MT = 5-methyltetrazole, IN = isonicotinic acid), [Zn(ET)(IN)] (**2**; ET = 5-ethyltetrazole), $[Zn(PT)_2]$ (**3**; PT = 5-propyltetrazole), and $[Zn(IPT)_2]$ (**4**; IPT = 5-isopropyltetrazole), have been obtained by in situ tetrazole synthesis and structurally characterized by elemental analyses, FTIR spectroscopy, and thermal studies, as well as by single-crystal and powder X-ray diffraction analyses. Compound **1** exhibits a two-fold diamondoid network constructed of two-dimensional (2D) Zn–MT wheel layers and IN linkers. Compound **2** displays a similar two-fold diamondoid network constructed by interconnection of Zn–ET–IN honeycomb layers and IN ligands. Compound **3** represents a 3D coordination polymer constructed from numerous $Zn_6(PT)_6$ wheels with a diamondoid net. Compound **4** is a 2D network constructed by the self-assembly of Zn ions and IPT ligands with an sql net. Furthermore, the solid-state properties of these crystalline materials, such as their thermal behavior and photoluminescence properties, have also been investigated.

Introduction

Recently, there has been growing interest in the study of metal–organic hybrid compounds, not only because of their intriguing structural architectures and topologies but also for their potential applications as functional materials in the fields of molecular recognition, ion exchange, adsorption, fluorescence, catalysis, and magnetism.[1–4] Self-assembly processes regulated by metal–ligand ligation have been widely exploited in the construction of metal–organic frameworks (MOFs), which has witnessed rapid progress over recent years. Up to now, considerable effort has been directed towards the synthesis of distinctive coordination polymers based upon carboxylate and/or pyridine-based ligands.[5] There are also many examples based upon polydentate aromatic nitrogen heterocyclic ligands or their derivatives, such as pyrazoles, imidazoles, and triazoles.[6]

Since the first tetrazole complex was discovered by Bladin,[7] tetrazole functional groups have been extensively used in coordination chemistry, medicinal chemistry, and materials science. Owing to their multiple N-donor atoms and various coordination modes, tetrazole and its derivatives have potential importance as functional ligands in coordination chemistry and crystal engineering. Since Demko and Sharpless described a safe, convenient, and environmentally friendly route to the synthesis of 5-substituted 1*H*-tetrazole complexes with zinc salt as a catalyst in water,[8] and especially since Xiong and co-workers[9] prepared a series of 5-substituted 1*H*-tetrazole complexes by an in situ hydrothermal method, the number of tetrazole-based coordination networks has grown dramatically. Although numerous tetrazole-based coordination networks have been extensively investigated,[10] to the best of our knowledge few entangled systems involving in situ tetrazole ligands have been reported.[11]

In our continuing studies of in situ ligand solvo/hydrothermal synthesis of metal tetrazolate complexes,[12] in this work we chose acetonitrile, propionitrile, butyronitrile, and isobutyronitrile, sodium azide, and isonicotinic acid (IN) with zinc salts as catalysts to synthesize metal–organic coordination networks for several reasons. (1) The zinc ion is not only able to support various coordination numbers, but also shows luminescent properties when coordinated to functional ligands.[13] (2) Tetrazole with its four nitrogen atoms permits a range of versatile bridging modes and is synthesized through an in situ route that is safe, convenient, and environmentally friendly. (3) Substituents at the 5-position of tetrazole play an important role in the growth of coordination frameworks and their variation influences the structural topologies of the resultant frameworks.[14] (4) The IN ligand, which possesses both a pyridyl nitrogen atom and carboxy oxygen atoms, is a good potential spacer for the construction of novel frameworks with large voids or entanglement.[15]

On the basis of these points, the aim of this research was to synthesize in situ novel tetrazole-based coordination polymers with interesting structural topologies and excellent physicochemical properties. Recently, we embarked on a systematic investigation of the effect of tetrazoles with

[a] School of Chemistry & Environment and Key Laboratory of Electrochemical Technology on Energy Storage and Power Generation in Guangdong Universities, South China Normal University,
Guangzhou 510006, China
E-mail: dh@scnu.edu.cn

Supporting information for this article is available on the WWW under http://dx.doi.org/10.1002/ejic.201100213.

different substituents at the 5-position on the construction of coordination polymers.[12d] To extend the study of structural assemblies we used four different organic nitriles RCN [R = CH_3, CH_3CH_2, $CH_3CH_2CH_2$, and $(CH_3)_2CH$] along with a functional co-ligand of isonicotinic acid to construct zinc coordination polymers through in situ tetrazole synthesis. In addition, the thermal stability and solid-state photofluorescent properties of these zinc coordination polymers have also been explored.

Results and Discussion

Syntheses

The four zinc–tetrazole coordination frameworks **1**–**4** were obtained by the hydrothermal reaction of nitriles (RCN), sodium azide, and the IN ligand with the aid of zinc salts (Scheme 1). In our synthesis, as expected, with the help of the IN ligands, compounds **1** and **2** formed two-fold interpenetrating coordination frameworks. However, compounds **3** and **4** did not co-ligate with IN ligands, which can be attributed to the large steric hindrance of the alkyl chains in the PT and IPT ligands (details will be given in the Crystal Structure Characterization section). Interestingly, all the tetrazole groups in the four compounds exhibited μ_2-bridging modes through two nitrogen atoms coordinated to two metal ions (Scheme 2): (I) Coordination mode observed in compounds **1**–**3** and (II) coordination mode observed in compound **4**.

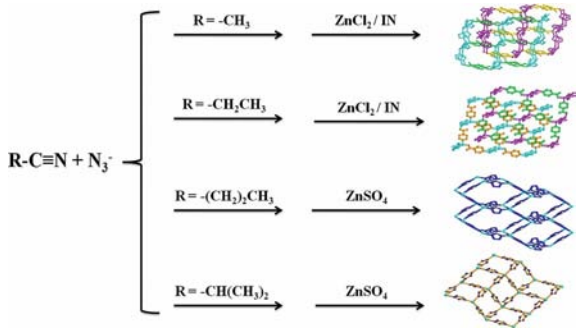

Scheme 1. In situ hydrothermal synthetic strategy for **1**–**4**.

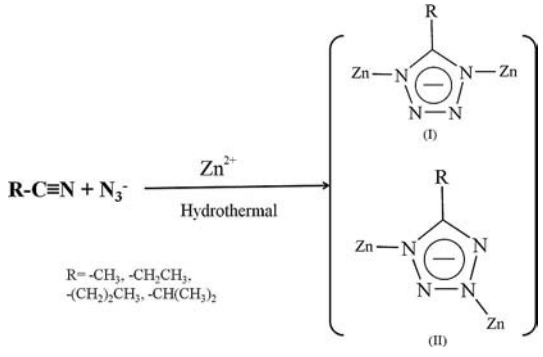

Scheme 2. In situ hydrothermal syntheses of compounds and their coordination modes. (I) Binding mode observed in compounds **1**–**3** and (II) binding mode observed in compound **4**.

Crystal Structure Characterization

Crystal Structure of [$Zn_2(MT)_3(IN)$] (1)

Compound **1** is a two-fold diamondoid network with two self-penetrating nets constructed from two-dimensional (2D) Zn–MT honeycomb layers and IN linkers and crystallizing in the monoclinic space group $P2_1/c$. As shown in Figure 1a, the asymmetric unit of **1** contains two crystallographically independent Zn^{II} ions, three MT ligands, and one IN ligand. Both Zn^{II} ions exhibit tetrahedral coordination, the Zn1 center is coordinated by three nitrogen atoms from three different MT ligands and one oxygen atom from the carboxy group of the IN ligand, whereas the Zn2 center is coordinated by four nitrogen atoms, three of them coming from three MT ligands and the fourth coming from the pyridine ring of the IN ligand. The Zn–N and Zn–O bond lengths range from 1.949(2) to 2.011(3) Å, and the N–Zn–N and N–Zn–O bond angles fall between 99.57(1) and 119.84(1)°. All of the tetrazole groups coordinated to the two Zn^{II} ions are involved in μ_2-N^1,N^4 bridging, whereas the IN ligand is also involved in bridging coordination, the nitrogen atom of the pyridine ring linking one Zn^{II} ion and one oxygen atom of the carboxy group connecting another Zn^{II} ion.

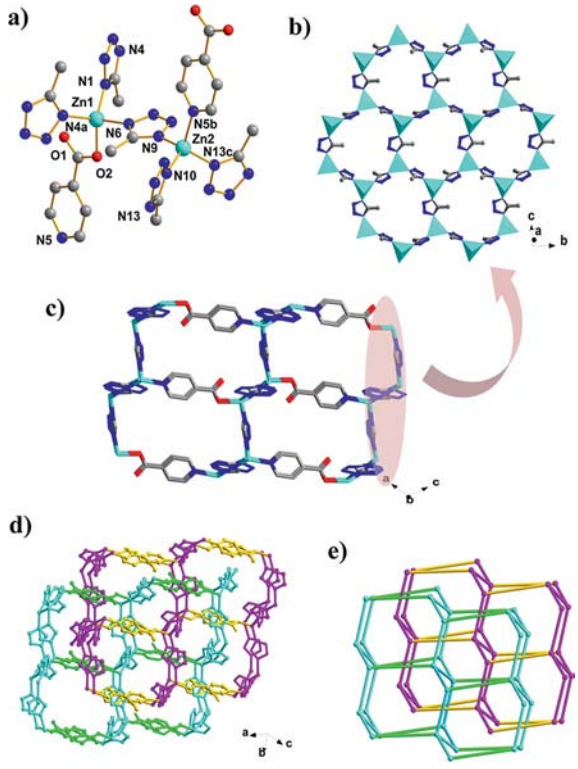

Figure 1. (a) View of the asymmetric unit of structure **1**. (b) View of the 2D Zn–MT honeycomb layer along the *ab* plane. (c) View of the single 3D net of compound **1**. (d) View of the two-fold network of complex **1**. (e) View of the two-fold diamond net when each Zn^{II} ion is taken as a node. (All H atoms have been omitted for clarity; N atoms are represented as blue spheres, C as gray, O as red, and Zn as cyan.) Symmetry transformations: a: 2 – *x*, 0.5 + *y*, 2.5 – *z*; b: –1 + *x*, *y*, *z*; c: 1 – *x*, –0.5 + *y*, 1.5 – *z*.

Note that the structure of **1** contains a nanosized Zn_6MT_6 honeycomb, which is constructed by the interconnection of Zn^{II} ions and MT ligands. The diameter of the wheel is approximately 10.4 Å. Each wheel is further linked to adjacent wheels by sharing two neighboring Zn^{II} ions with a Zn···Zn separation of around 6.1 Å, leading to a highly ordered (6,3) honeycomb-layered sheet (Figure 1b). Moreover, these sheets form pillars through the interactions of the rigid IN ligands, thereby forming a 3D framework with dimensions of $9.6 \times 10.4 \times 12.0$ Å (Figure 1c). The single net of **1** possesses large channels that can be filled with solvents or be penetrated by other nets to consolidate the stability of the frameworks. In this case, two 3D networks self-penetrate to furnish this two-fold interpenetration leaving nearly no residual accessible void (calculated by the PLATON program;[16] Figure 1d). To better understand the nature of the intricate framework, a topological approach to simplify the 3D structures can be accomplished by reducing them to simple nodes and links. Thus, if the tetrahedral Zn^{II} centers are regarded as four-connected nodes and the MT and IN ligands are simplified to the links of a topological network, the 3D framework of **1** can be seen in a simplified way as a two-fold interpenetrating diamondoid net with Schläfli symbol (6^6) (Figure 1e).

Crystal Structure of [Zn(ET)(IN)] (2)

Complex **2** has a very similar two-fold interpenetrating network as complex **1** constructed by the interconnection of numerous Zn–ET and Zn–IN chains. Compound **2** is monoclinic with space group *C*2/*c*. As shown in Figure 2a, the asymmetric unit contains one crystallographically independent Zn^{II} ion, one ET ligand, and one IN ligand. Each Zn^{II} ion is coordinated by three nitrogen atoms from two different ET ligands and one IN ligand and by one oxygen atom from the carboxy group of the IN ligand in a slightly distorted tetrahedron coordination environment. The Zn–N bond lengths fall between 1.994(3) and 2.059(2) Å, and the N–Zn–N bond angles range from 103.19(1) to 111.54(1)°. The Zn–O bond length is 1.940(2) Å, and the N–Zn–O bond angles range from 96.56(1) to 119.52(1)°. All of the tetrazole groups are involved in μ_2-N^1,N^4 bridging with two nitrogen atoms coordinating to two Zn^{II} ions, and the IN ligand is also involved in bridging coordination, with the pyridyl nitrogen atom and one carboxy oxygen atom coordinated to two Zn^{II} ions.

It is very interesting that the ET ligands bind to transition-metal Zn^{II} ions, forming an infinite zigzag Zn–ET chain running along the *c* axis (Figure S1). The Zn–Zn separation in the chain is approximately 6.11 Å. Such chains are interconnected through linear IN bridges to complete a 2D Zn–ET–IN wheel layer (Figure 2). The adjacent layers are connected to each other by IN linkers to form a 3D network with dimensions of $8.8 \times 10.2 \times 12.1$ Å (Figure 2c). Similarly to compound **1**, although the single net of **2** has large channels, they are mainly filled by another equivalent net (Figure 2d), leaving only small cavities [a total of 345.9 Å^3 (13.9% of the total cell volume calculated by the PLATON program[16])] in each unit cell without any solvent molecule in the lattice. If the Zn^{II} ions are considered as four-connected nodes and the ET and IN ligands both as links, the whole structure of **2** can also be described as a two-fold interpenetrating diamondoid net (Figure 2e).

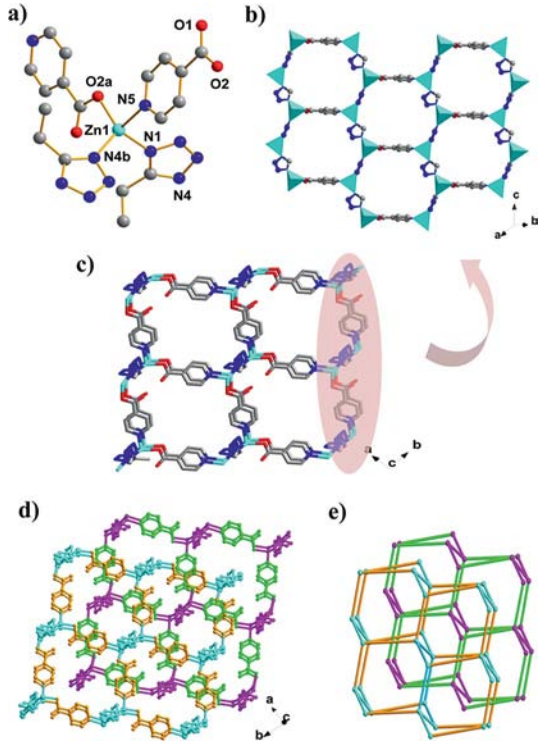

Figure 2. (a) View of the asymmetric unit of structure **2**. (b) View of the 2D Zn–ET–IN honeycomb layer along the *bc* plane. (c) View of the single 3D net of compound **2**. (d) View of the two-fold network of compound **2**. (e) View of the two-fold diamond net of complex. (All H atoms have been omitted for clarity; N atoms are represented as blue spheres, C as gray, O as red, Zn as cyan, and Cd as dark cyan.) Symmetry transformations: a: –0.5 + *x*, 0.5 – *y*, –0.5 + *z*; b: *x*, –*y*, 0.5 + *z*; c: *x*, –*y*, 0.5 + *z*; d: 0.5 + *x*, 0.5 – *y*, 0.5 + *z*.

Crystal Structure of [Zn(PT)$_2$] (3)

Compound **3** is a 3D coordination polymer constructed by the interconnection of Zn–PT subunits and characterized by the tetragonal noncentrosymmetric space group $I\bar{4}2d$ with a Flack parameter of 0.04(2). The propyl group of the PT ligand exhibits large disorder across a crystallographic mirror plane (see the Crystal Structure Determination section for details). As shown in Figure 3a, the asymmetric unit of **3** contains a quarter of a Zn^{II} ion and half a PT ligand. The Zn^{II} ion is coordinated by four nitrogen atoms from four different PT ligands to furnish a tetrahedron coordination environment. Each PT ligand passes across a two-fold axis and adopts the μ_2-N^1,N^4 bridging mode to connect two Zn^{II} ions with a Zn–Zn separation of approximately 6.08 Å.

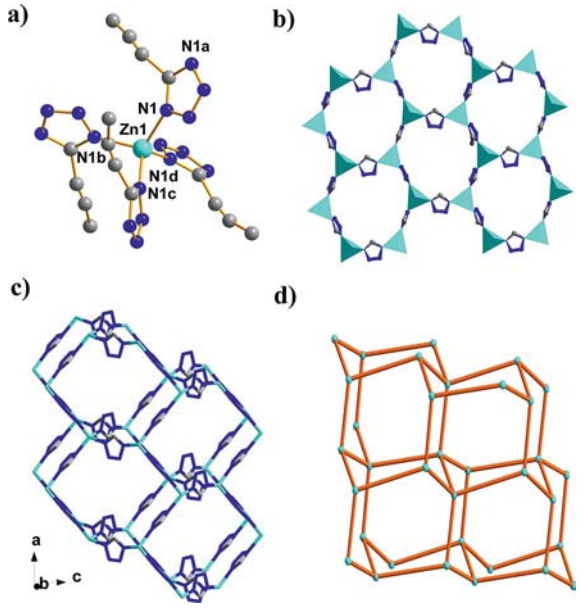

Figure 3. (a) View of the asymmetric unit of structure **3**. (b) View of the Zn–BT six-membered honeycomb layer. (c) View of the 3D network of **3**. (d) View of the diamond-like net generated by interconnection of the zinc tetrahedron. (All H atoms have been omitted for clarity; N atoms are represented as blue sphheres, C as gray, and Zn as cyan.) Symmetry transformations: a: x, 0.5 – y, 0.25 – z; b: y, $–x$, $–z$; c: $–y$, x, $–z$; d: $–x$, $–y$, z.

The most striking structural feature of **3** is the interlinking of six Zn^{II} ions by six PT ligands to generate a nanosized honeycomb similar to the Zn–MT honeycomb in **1** (Figure 3b). The diameter of the wheel is approximately 10.2 Å. The adjacent honeycombs are connected to each other by PT bridges to furnish a 3D network with dimensions of $10.2 \times 10.2 \times 10.2$ Å (Figure 3c). However, the large cavities are occupied by numerous disordered propyl groups. Topologically, if each of the Zn^{II} ions can be considered as four-connected nodes and the PT ligands as linkers, then the 3D network can be described as a diamond-like topological net with Schläfli symbol (6^6) (Figure 3d).

Crystal Structure of [Zn(IPT)$_2$] (4)

Single-crystal X-ray diffraction analysis revealed that structure **4** crystallizes in the orthorhombic space group *Pbca* and represents a 2D coordination framework constructed from the self-assembly of Zn ions and IPT ligands. As depicted in Figure 4a, the asymmetric unit of **4** contains one crystallographically independent Zn^{II} ion and two IPT ligands. Each Zn ion is coordinated by four nitrogen atoms from four different IPT ligands in a tetrahedral coordination geometry. The Zn–N bond lengths fall between 1.982(2) and 2.002(2) Å, and the N–Zn–N bond angles range from 101.50(9) to 116.16(9)°. Two crystallographically independent IPT ligands in **4** coordinate to two Zn^{II} ions through the μ_2-N^1,N^3 bridging mode.

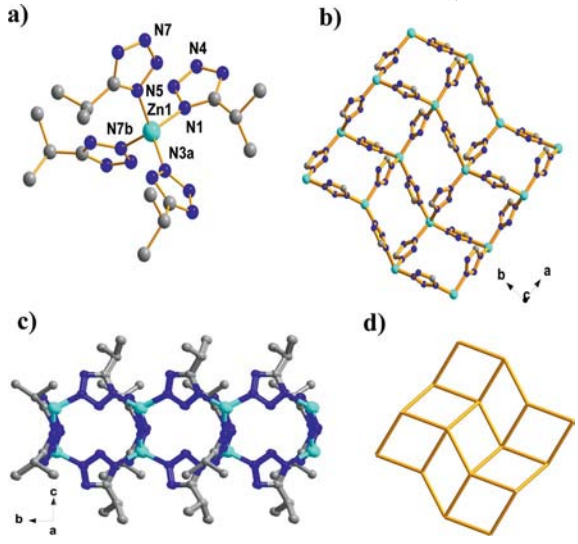

Figure 4. (a) View of the asymmetric unit of structure **4**. (b) View of the 2D Zn–IPT layer along the *ab* plane. (c) View of the Zn–IPT wheel along the *bc* plane. (d) View of the sql net generated by interconnection of the zinc tetrahedron. (All H atoms have been omitted for clarity; N atoms are represented as blue spheres, C as gray, and Zn as cyan.) Symmetry transformations: a: –0.5 + x, y, 0.5 – z; b: 0.5 – x, –0.5 + y, z.

In the structure of **4**, IPT ligands link Zn^{II} ions through the μ_2-N^1,N^3 bridging mode, giving rise to a 2D-layered network in the *ab* plane of the unit cell (Figure 4b). The 2D net contains numerous $Zn_4(IPT)_4$ wheels (Figure 4c). Topologically, the 2D network can be seen in a simplified way as an sql net with Schläfli symbol (4^4, 6^2) if the four coordination Zn^{II} ions are regarded as four-connected nodes and the IPT ligands as links (Figure 4d).

Influence of the 5-Substituted Groups and the IN Ligands

The structures of **1** and **2** both contain 2D honeycomb layers (see Figures 1b and 2b). The 2D layer in **1** is constructed of six Zn^{II} ions and six tetrazole-based MT ligands, whereas the 2D layer in **2** is constructed of six Zn^{II} ions, four tetrazole-based ET ligands, and two IN linkers. The difference originates from the steric hindrance of the alkyl chains between the terminal groups of the MT and ET ligands. For compound **1**, the void in the layer comprised of six Zn^{II} ions and MT ligands is large enough to allow an IN ligand to pass through vertically, whereas for compound **2** to form a large void that allows an IN ligand to pass through, two tetrazole ligands are spontaneously replaced by two IN ligands. To further tune the assembly of d^{10} metal ions and the in situ synthesis of tetrazole ligands, pore filling by appropriate solvents will be a solution to prohibit self-penetration of the network to construct open metal–organic frameworks. In addition, the open MOFs with nitrogen-free sites will be a functional material for enhancing CO_2 sorption capability or ion-sensing.[4d,4e,12b,12c] This experiment is currently underway in our laboratory.

Although the synthesis was performed under the same reaction conditions, IN ligands were not observed in compounds **3** and **4**. It is plausible that the presence of the dif-

ferent electron-donating alkyl groups [CH_3, CH_2CH_3, $(CH_2)_2CH_3$, and $CH(CH_3)_2$] result in Zn^{II} centers with different Lewis acidity. Moreover, the 5-alkyl substituents have different steric hindrances, in particular, the $(CH_2)_2CH_3$ and $CH(CH_3)_2$ groups have large steric hindrance. Thus, the structural diversity may be attributed to electronic and/or steric effects of the ligands.[17] In the crystal structures of **1** and **3** (see Figures 1b and 3b), similar 2D nets both containing six Zn^{II} ions and six tetrazole-based ligands are observed. The long alkyl chains of the PT ligands point into the channels, and, although leaving a total of 58.5 Å^3 void in each unit cell (4.3% of the total cell volume calculated by the PLATON program[16]), the void is not large enough for the interpenetration of any networks.

Each grid in the 2D net of compound **4** contains only four Zn^{II} ions and four tetrazole-based ligands. Its form is distinct from those of compounds **1**–**3**, which is probably a result of electronic and/or steric effects of the IPT ligands. The large steric hindrance of IPT leads to the formation of a 2D layered network.

Thermal Analyses and Powder X-ray Diffraction Measurements

Thermogravimetric analyses (TGA) of all four complexes were undertaken in the temperature range 35–750 °C at a heating rate of 10 °C/min in dry air to study their thermal behavior. As shown in Figure S2 of the Supporting Information, the TGA curves of the compounds reveal that they are stable up to approximately 300 °C, whereas above these temperatures their networks start to decompose. Simulated and experimental powder X-ray diffraction (PXRD) patterns of **1**–**4** are shown in Figures 5 and S3. All the peaks presented in the recorded curves closely match those in the simulated curves generated from single-crystal diffraction data, which clearly confirms the phase purity of the as-prepared products.

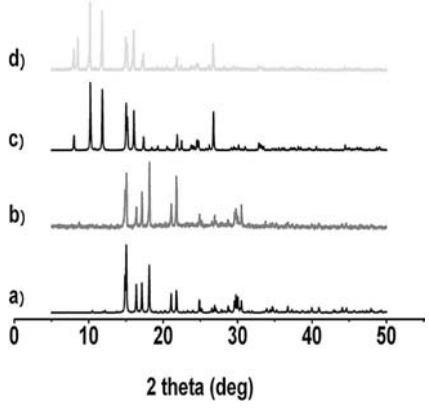

Figure 5. PXRD patterns: (a) simulated based on the X-ray single-crystal diffraction date of **1**, (b) of as-synthesized **1**, (c) simulated based on the X-ray single-crystal diffraction date of **2**, and (d) of as-synthesized **2**.

Spectroscopic Studies

The absorption bands at 3100–3030 cm^{-1} in the FTIR spectra of compounds **1**–**4** can be ascribed to the C–H stretching vibrations of the pyridine ring, whereas the ν_{C-H} bands of $-CH_3$ and $-CH_2$ appear in the region 2986–2860 cm^{-1}. Although the emergence of peaks in the 1400–1500 cm^{-1} region clearly confirms the formation of tetrazole groups, the bands at 1634–1636 and 1560 cm^{-1} for compounds **1** and **2** are associated with asymmetric and symmetric COO– stretching, respectively.

Owing to the excellent luminescence properties of zinc complexes, the luminescence of the complexes **1**–**4** was investigated in the solid state at room temperature (Figure 6). Their emission spectra have broad peaks with maxima at 397, 443, 447, and 410 nm for complexes **1**–**4** with excitation at 356, 331, 370, and 357 nm, respectively, and the lifetimes of compounds **1**–**4** are 12.35, 10.43, 3.58, and 4.86 ns, respectively. From literature reports, the free tetrazole ligand presents a very weak photoluminescence emission centered at 325 nm at room temperature.[18] Therefore, the strong fluorescence emissions and distinct redshifts of **1**–**4** may be ascribed to the cooperative effects of intraligand emission and ligand-to-metal charge transfer (LMCT).[18,19] The emission of compound **1** (397 nm) is blueshifted relative to the emissions of **2**–**4** (410–447 nm). In addition, its lifetime is longer than those of compounds **2**–**4**, which may be due to their long flexible alkyl chains with stronger vibrations of the frameworks and more radiationless energy decay. The variations in the photoluminescence of these compounds and their lifetimes may be attributed to the different substituents at the 5-position of the tetrazole ligands of zinc ions and/or their local coordination environments. These emission bands in the blue region suggest that these complexes may be potential candidates for blue-light-emitting materials.

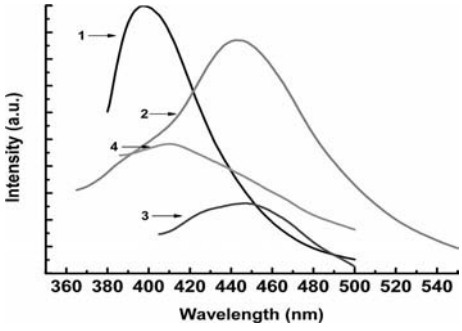

Figure 6. Luminescence curves of compounds **1**–**4**.

Conclusion

We have obtained four zinc–tetrazole-based coordination complexes by in situ tetrazole synthesis under hydrothermal conditions by employing zinc salts, organic nitriles, azide anions, and isonicotinic acid ligands. Owing to the different steric hindrances of the in situ formed tetrazole ligands, the four compounds form diverse frameworks: Compounds **1** and **2** form similar two-fold diamondoid networks, compound **3** is a noninterpenetrating diamondoid framework, and compound **4** is a 2D sql net. In addition, all the syn-

thetic crystalline materials have high thermal stability and are potential candidates for photoactive materials. We believe that the synthetic strategies adopted in this work will prevail in the preparation of other novel tetrazole–metal coordination networks with interesting structural and functional properties.

Experimental Section

Materials and Instruments: All the materials and reagents were obtained commercially and used without further purification. Elemental (C, H, N) analyses were performed with a Perkin–Elmer 2400 element analyzer. Infrared (IR) samples were prepared as KBr pellets, and spectra were obtained in the 4000–400 cm^{-1} range by using a Nicolet Avatar 360 FT-IR spectrophotometer. Thermogravimetric analyses (TGA) were carried out with a Perkin–Elmer TGA 7 thermogravimetric analyzer at a heating rate of 10 °C/min from 35 to 750 °C under dry air. Powder XRD investigations were performed with a Philips PW-1830 X-ray diffractometer with Cu-K_α radiation. Fluorescence spectra were recorded with an Edinburgh FLS920 spectrophotometer analyzer.

Single-Crystal Structure Determination: Single-crystal X-ray diffraction data collections of **1**–**4** were performed with a Bruker Apex II CCD diffractometer operating at 50 kV and 30 mA by using Mo-K_α radiation (λ = 0.71073 Å). Data collection and reduction were performed by using the APEX II software.[20a] Multi-scan absorption corrections were applied to all the data sets by using the APEX II program.[20a] The structures were solved by direct methods and refined by full-matrix least squares on F^2 by using the SHELXTL program package.[20b] All non-hydrogen atoms were refined with anisotropic displacement parameters. Hydrogen atoms attached to carbon atoms were placed in geometrically idealized positions and refined by using a riding model. Hydrogen atoms of water molecules were located from difference Fourier maps and were also refined by using a riding model. Each of the terminal propyl groups of the highly symmetrical compound **3** is disordered; the disorder was refined with a "part –1" order. Selected bond lengths and angles are given in Table 1 and the crystallographic data for complexes **1**–**4** are listed in Table 2. The lengths [Å] and angles [°] of the hydrogen bonds in complexes **1**–**4** are listed in Table S1 in the Supporting Information. CCDC-793774 (for **1**), -793775 (for **2**), -795095 (for **3**), and -795096 (for **4**) contain the supplementary crystallographic data for this paper. These data can be obtained free of charge from The Cambridge Crystallographic Data Centre via www.ccdc.cam.ac.uk/data_request/cif.

Synthesis of $[Zn_2(MT)_3(IN)]$ (1): An aqueous mixture (10.0 mL) of CH_3CN (2.0 mL), $ZnCl_2$ (0.136 g, 1.0 mmol), IN (0.062 g, 0.5 mmol), and NaN_3 (0.065 g, 1.0 mmol) was placed in a 23.0 mL Teflon-lined stainless-steel autoclave and heated at 150 °C for 3 d and then cooled to room temperature at 5 °C/h. Colorless prismatic single crystals of **1** were obtained (yield: 0.100 g, 40% based on Zn). IR (KBr): $\tilde{\nu}$ = 3094 (w), 3069 (w), 2986 (w), 2861 (w), 1634 (s), 1560 (m), 1500 (m), 1389 (s), 1107 (w), 1060 (m) cm^{-1}. $C_{12}H_{13}N_{13}O_2Zn_2$ (502.13): calcd. C 28.70, H 2.61, N 36.26; found C 28.65, H 2.70, N 36.32.

Synthesis of [Zn(ET)(IN)] (2): An aqueous mixture (10.0 mL) of CH_3CH_2CN (2.0 mL), $ZnCl_2$ (0.136 g, 1.0 mmol), IN (0.062 g, 0.5 mmol), and NaN_3 (0.065 g, 1.0 mmol) was placed in a 23 mL Teflon-lined stainless-steel autoclave and heated at 150 °C for 3 d and then cooled to room temperature at 5 °C/h. Colorless, octahedral single crystals of **2** were obtained (yield: 0.219 g, 77% based on Zn). IR (KBr): $\tilde{\nu}$ = 3100 (w), 3052 (w), 2977 (m), 2880 (w), 1636 (s), 1560 (m), 1496 (m), 1425 (s), 1370 (s), 1077 (m) cm^{-1}. $C_9H_9N_5O_2Zn$ (284.60): calcd. C 37.98, H 3.19, N 24.61; found C 37.91, H 3.23, N 24.55.

Table 1. Selected bond lengths [Å] and angles [°] for complexes **1**–**4**. Symmetry transformations used to generate equivalent atoms are given as footnotes.

Compound **1**[a]			
N(1)–Zn(1)	1.992(3)	O(2)–Zn(1)–N(1)	119.84(11)
N(4)–Zn(1)#1	2.001(3)	O(2)–Zn(1)–N(4)#4	109.10(11)
N(5)–Zn(2)#2	2.011(3)	N(1)–Zn(1)–N(4)#4	113.57(12)
N(6)–Zn(1)	2.023(3)	O(2)–Zn(1)–N(6)	99.57(11)
N(9)–Zn(2)	2.001(3)	N(1)–Zn(1)–N(6)	104.52(11)
N(10)–Zn(2)	1.987(3)	N(4)#4-Zn(1)–N(6)	108.67(11)
N(13)–Zn(2)#3	2.000(3)	N(10)–Zn(2)–N(13)#5	114.92(11)
O(2)–Zn(1)	1.949(2)	N(10)–Zn(2)–N(9)	115.53(11)
Zn(1)–N(4)#4	2.001(3)	N(13)#5-Zn(2)–N(9)	101.14(11)
Zn(2)–N(13)#5	2.000(3)	N(10)–Zn(2)–N(5)#6	106.76(11)
Zn(2)–N(5)#6	2.011(3)	N(13)#5–Zn(2)–N(5)#6	112.82(11)
C(3)–O(2)–Zn(1)	109.0(2)	N(9)–Zn(2)–N(5)#6	105.40(12)
Compound **2**[b]			
Zn(1)–O(2)#1	1.940(2)	O(2)#1–Zn(1)–N(4)#2	119.52(10)
Zn(1)–N(4)#2	1.994(3)	O(2)#1–Zn(1)–N(1)	117.01(11)
Zn(1)–N(1)	2.002(3)	N(4)#2–Zn(1)–N(1)	111.54(11)
Zn(1)–N(5)	2.059(2)	O(2)#1–Zn(1)–N(5)	96.56(10)
O(2)–Zn(1)#3	1.940(2)	N(4)#2–Zn(1)–N(5)	105.45(10)
N(4)–Zn(1)#4	1.994(3)	N(1)–Zn(1)–N(5)	103.19(10)
Compound **3**[c]			
Zn(1)–N(1)#1	1.9913(1)	N(1)#1–Zn(1)–N(1)#2	111.59(4)
Zn(1)–N(1)	1.9913(1)	N(1)–Zn(1)–N(1)#2	105.32(8)
Zn(1)–N(1)#2	1.9913(1)	N(1)#1–Zn(1)–N(1)#3	105.32(8)
Zn(1)–N(1)#3	1.9913(1)	N(1)–Zn(1)–N(1)#3	111.59(4)
Compound **4**[d]			
Zn(1)–N(3)#1	1.982(2)	N(3)#1–Zn(1)–N(7)#2	112.67(9)
Zn(1)–N(7)#2	1.988(2)	N(3)#1–Zn(1)–N(5)	106.97(9)
Zn(1)–N(5)	1.999(2)	N(7)#2–Zn(1)–N(5)	114.47(9)
Zn(1)–N(1)	2.002(2)	N(3)#1–Zn(1)–N(1)	116.16(9)
N(3)–Zn(1)#3	1.982(2)	N(7)#2–Zn(1)–N(1)	104.79(9)
N(7)–Zn(1)#4	1.988(2)	N(5)–Zn(1)–N(1)	101.50(9)

[a] #1: $-x + 2$, $y - 1/2$, $-z + 5/2$; #2: $x + 1$, y, z; #3: $-x + 1$, $y + 1/2$, $-z + 3/2$; #4: $-x + 2$, $y + 1/2$, $-z + 5/2$; #5: $-x + 1$, $y - 1/2$, $-z + 3/2$; #6: $x - 1$, y, z. [b] #1: $x - 1/2$, $-y + 1/2$, $z - 1/2$; #2: x, $-y$, $z + 1/2$; #3: $x + 1/2$, $-y + 1/2$, $z + 1/2$; #4: x, $-y$, $z - 1/2$. [c] #1: $-y$, x, $-z$; #2: $-x$, $-y$, z; #3: y, $-x$, $-z$. [d] #1: $x - 1/2$, y, $-z + 1/2$; #2: $-x + 1/2$, $y - 1/2$, z; #3: $x + 1/2$, y, $-z + 1/2$; #4: $-x + 1/2$, $y + 1/2$, z.

Synthesis of $[Zn(PT)_2]$ (3): An aqueous mixture (10.0 mL) of $CH_3CH_2CH_2CN$ (2.0 mL), $ZnSO_4$ (0.161 g, 1.0 mmol), IN (0.062 g, 0.5 mmol), and NaN_3 (0.065 g, 1.0 mmol) was placed in a 23 mL Teflon-lined stainless-steel autoclave and heated at 150 °C for 3 d and then cooled to room temperature at 5 °C/h. Colorless, block single crystals of **4** were obtained (yield: 0.195 g, 68% based on Zn). IR (KBr): $\tilde{\nu}$ = 2969 (s), 2875 (m), 1493 (s), 1429 (s), 1282 (m), 1083 (m), 1064 (m), 1022 (w), 897 (w), 701 (w) cm^{-1}. $C_8H_{14}N_8Zn$ (287.66): calcd. C 33.40, H 4.91, N 38.95; found C 33.46, H 4.98, N 38.84.

Synthesis of $[Zn(IPT)_2]$ (4): An aqueous mixture (10.0 mL) of $(CH_3)_2CHCN$ (2.0 mL), $ZnSO_4$ (0.161 g, 1.0 mmol), IN (0.062 g, 0.5 mmol), and NaN_3 (0.065 g, 1.0 mmol) was placed in a 23 mL Teflon-lined stainless-steel autoclave and heated at 150 °C for 3 d and then cooled to room temperature at 5 °C/h. Colorless, block

Table 2. Crystal data for the structure determinations of complexes **1**–**4**.

	1	**2**	**3**	**4**
Empirical formula	$C_{12}H_{13}N_{13}O_2Zn_2$	$C_9H_9N_5O_2Zn$	$C_8H_{14}N_8Zn$	$C_8H_{14}N_8Zn$
Formula mass	502.13	284.60	287.66	287.66
T [K]	296	296	296	296
Crystal system	monoclinic	monoclinic	tetragonal	orthorhombic
Space group	$P2_1/c$	$C2/c$	$I\text{-}42d$	$Pbca$
a [Å]	12.396(2)	17.910(3)	9.3723(7)	9.9377(3)
b [Å]	10.3373(17)	16.295(3)	9.3723(7)	10.6391(3)
c [Å]	15.128(3)	10.2009(18)	15.518(2)	24.0171(8)
β [°]	106.259(2)	123.401(2)	90	90
V [$Å^3$]	1861.0(6)	2485.4(8)	1363.1(2)	2539.28(13)
Z	4	8	4	8
$\rho_{calcd.}$ [$g\,cm^3$]	1.792	1.521	1.402	1.505
μ [mm^{-1}]	2.619	1.974	1.795	1.927
$F(000)$	1008.0	1152.0	592.0	1184.0
GOF	1.007	1.045	1.051	1.060
$R_1[I>2\sigma(I)]$[a]	0.0329	0.0317	0.0158	0.0316
wR_2 (all data)[b]	0.0745	0.0848	0.0402	0.0737

[a] $R1 = \Sigma||F_o| - |F_c||/\Sigma|F_o|$. [b] $wR2 = [\Sigma w(F_o^2 - F_c^2)^2/\Sigma w(F_o^2)^2]^{1/2}$.

single crystals of **5** were obtained (yield: 0.155 g, 54% based on Zn). IR (KBr): $\tilde{\nu}$ = 2979 (s), 2936 (m), 2874 (w), 1493 (s), 1415 (m), 1291 (s), 1148 (s), 1111 (m), 1072 (s), 665 (m) cm^{-1}. $C_8H_{14}N_8Zn$ (287.66): calcd. C 33.40, H 4.91, N 38.95; found C 33.48, H 4.97, N 38.89.

Supporting Information (see footnote on the first page of this article): The Zn–ET chain of compound **2** (Figure S1), the TGA curves of compounds **1**–**4** (Figure S2), the PXRD patterns of compounds **3** and **4** (Figure S3) and distances [Å] and angles [°] of hydrogen bonds for complexes **1**–**4** (Table S3).

Acknowledgments

This work was supported by the National Natural Science Foundation of China (Grant No. 20871048).

[1] a) M. Eddaoudi, D. B. Moler, H. Li, B. Chen, T. M. Reineke, M. O'Keeffe, O. M. Yaghi, *Acc. Chem. Res.* **2001**, *34*, 319–330; b) J. L. C. Rowsell, O. M. Yaghi, *Microporous Mesoporous Mater.* **2004**, *73*, 3–14; c) S. Kitagawa, R. Kitaura, S. Noro, *Angew. Chem. Int. Ed.* **2004**, *43*, 2334–2375; d) B. Moulton, M. J. Zaworotko, *Chem. Rev.* **2001**, *101*, 1629–1658.

[2] a) M. W. Hosseini, *Acc. Chem. Res.* **2005**, *38*, 313–323; b) D. Dubbeldam, C. J. Galvin, K. S. Walton, D. E. Ellis, R. Q. Snurr, *J. Am. Chem. Soc.* **2008**, *130*, 10884–10885; c) J. S. Seo, D. Whang, H. Lee, S. I. Jun, J. Oh, Y. J. Jeon, K. Kim, *Nature* **2000**, *404*, 982–986; d) L. Pan, D. H. Olson, L. R. Ciemnolonski, R. Heddy, J. Li, *Angew. Chem. Int. Ed.* **2006**, *45*, 616–619; e) B. L. Chen, C. D. Liang, J. Yang, D. S. Contreras, Y. L. Clancy, E. B. Lobkovsky, O. M. Yaghi, S. Dai, *Angew. Chem. Int. Ed.* **2006**, *45*, 1390–1393.

[3] a) A. Y. Robin, K. M. Fromm, *Coord. Chem. Rev.* **2006**, *250*, 2127–2157; b) L. Carlucci, G. Ciani, D. M. Prosperio, *Coord. Chem. Rev.* **2003**, *246*, 247–289; c) S. R. Batten, R. Robson, *Angew. Chem. Int. Ed.* **1998**, *37*, 1461–1494; d) A. B. Gaspar, V. Ksenofontov, M. Seredyuk, P. Guetlich, *Coord. Chem. Rev.* **2005**, *249*, 2661–2676; e) Y. Cui, O. R. Evans, H. L. Ngo, P. S. White, W. Lin, *Angew. Chem. Int. Ed.* **2002**, *41*, 1159–1162.

[4] a) R. Vaidhyanathan, D. Bradshaw, J. N. Rebilly, J. P. Barrio, J. A. Gould, N. G. Berry, M. J. Rosseinsky, *Angew. Chem. Int. Ed.* **2006**, *45*, 6495–6499; b) B. Kesanli, W. Lin, *Coord. Chem. Rev.* **2003**, *246*, 305–326; c) C. D. Wu, W. Lin, *Chem. Commun.* **2006**, 3673–3675; d) Y. C. Qiu, Z. H. Liu, Y. H. Li, H. Deng, R. H. Zeng, M. Zeller, *Inorg. Chem.* **2008**, *47*, 5122–5128; e) B. Wang, A. P. Cote, H. Furukawa, M. O'Keeffe, O. M. Yaghi, *Nature* **2008**, *453*, 207–211; f) H. Deng, Y. C. Qiu, C. Daiguebonne, N. Kerbellec, O. Guillou, M. Zeller, S. R. Batten, *Inorg. Chem.* **2008**, *47*, 5866–5872.

[5] a) C. N. R. Rao, S. Natarajan, R. Vaidhzanathan, *Angew. Chem. Int. Ed.* **2004**, *43*, 1466–1496; b) S. S. Y. Chui, S. M. F. Lo, J. P. H. Charamant, A. G. Orpen, I. D. Williams, *Science* **1999**, *283*, 1148–1150; c) M. H. Zeng, B. Wang, X. Y. Wang, W. X. Zhang, X. M. Chen, S. Gao, *Inorg. Chem.* **2006**, *45*, 7069–7076.

[6] a) J. P. Zhang, Y. Y. Lin, W. X. Zhang, X. M. Chen, *J. Am. Chem. Soc.* **2005**, *127*, 14162–14163; b) Y. Wang, B. Ding, P. Cheng, D. Z. Liao, S. P. Yan, *Inorg. Chem.* **2007**, *46*, 2002–2010; c) J. P. Zhang, X. M. Chen, *Chem. Commun.* **2006**, 1689–1699.

[7] a) V. A. Ostrovskii, A. O. Koren, *Heterocycles* **2000**, *53*, 1421–1448; b) M. M. Harding, G. Mokdsi, *Curr. Med. Chem.* **2000**, *7*, 1289–1303; c) J. A. Bladin, *Ber. Dtsch. Chem. Ges.* **1885**, *18*, 1544–1551; d) H. Zhao, Z. R. Qu, H. Y. Ye, R. G. Xiong, *Chem. Soc. Rev.* **2008**, *37*, 84–100.

[8] a) Z. P. Demko, K. B. Sharpless, *J. Org. Chem.* **2001**, *66*, 7945–7950; b) Z. P. Demko, K. B. Sharpless, *Org. Lett.* **2001**, *3*, 4091–4094; c) Z. P. Demko, K. B. Sharpless, *Angew. Chem. Int. Ed.* **2002**, *12*, 2110–2113.

[9] a) R. G. Xiong, X. Xue, H. Zhao, X. Z. You, B. F. Abrahams, Z. L. Xue, *Angew. Chem. Int. Ed.* **2002**, *41*, 3800–3803; b) X. Xue, X. S. Wang, L. Z. Wang, R. G. Xiong, B. F. Abrahams, X. Z. You, Z. L. Xue, C. H. Che, *Inorg. Chem.* **2002**, *41*, 6544–6546; c) X. S. Wang, Y. Z. Tang, X. F. Huang, Z. R. Qu, C. M. Che, W. H. Chan, R. G. Xiong, *Inorg. Chem.* **2005**, *44*, 5278–5285.

[10] a) B. Liu, Y. C. Qiu, G. Peng, L. Ma, L. M. Jin, J. B. Cai, H. Deng, *Inorg. Chem. Commun.* **2009**, *12*, 1200–1203; b) P. Cui, Z. Chen, D. L. Gao, B. Zhao, W. Shi, P. Cheng, *Cryst. Growth Des.* **2010**, *10*, 4370–4378; c) J. Y. Zhang, A. L. Cheng, Q. Sun, Q. Yue, E. Q. Gao, *Cryst. Growth Des.* **2010**, *10*, 2908–2915.

[11] Y. W. Li, W. L. Chen, Y. H. Wang, Y. G. Li, E. B. Wang, *J. Solid State Chem.* **2009**, *182*, 736–743.

[12] a) H. Deng, Y. C. Qiu, Y. H. Li, Z. H. Liu, R. H. Zeng, M. Zeller, S. R. Batten, *Chem. Commun.* **2008**, 2239–2241; b) Y. C. Qiu, H. Deng, S. H. Yang, J. X. Mou, M. Zeller, S. R. Batten, H. H. Wu, J. Li, *Chem. Commun.* **2009**, 5415–5417; c) Y. C. Qiu, H. Deng, S. H. Yang, J. X. Mou, C. Daiguebonne, N. Kerbellec, O. Guillou, S. R. Batten, *Inorg. Chem.* **2009**, *48*, 3976–3981; d) Y. C. Qiu, Y. H. Li, G. Peng, J. B. Cai, L. M. Jin, L. Ma, H. Deng, M. Zeller, S. R. Batten, *Cryst. Growth Des.* **2010**, *10*, 1332–1340.

[13] a) L. Yi, B. Ding, P. Cheng, D. Z. Liao, S. P. Yan, Z. H. Jiang, *Inorg. Chem.* **2004**, *43*, 33–38; b) Y. L. Yao, L. Xue, Y. X. Che, J. M. Zheng, *Cryst. Growth Des.* **2009**, *9*, 606–610.
[14] a) G. Ferey, C. Mellot-Draznieks, C. Serre, F. Millange, *Acc. Chem. Res.* **2005**, *38*, 217–225; b) D. Bradshaw, J. B. Claridge, E. J. Cussen, T. J. Prior, M. Rosseinsky, *Acc. Chem. Res.* **2005**, *38*, 273–282; c) W. C. Song, J. R. Li, P. C. Song, Y. Tao, Q. Yu, X. L. Tong, X. H. Bu, *Inorg. Chem.* **2009**, *48*, 3792–3799; d) J. R. Li, Y. Tao, Q. Yu, X. H. Bu, *Chem. Commun.* **2007**, 1527–1529; e) J. R. Li, Y. Tao, Q. Yu, X. H. Bu, H. Sakamoto, S. Kitagawa, *Chem. Eur. J.* **2008**, *14*, 2771–2776; f) S. M. Zhang, Z. Chang, T. L. Hu, X. H. Bu, *Inorg. Chem.* **2010**, *49*, 11581–11586; g) X. L. Tong, D. Z. Wang, T. L. Hu, W. C. Song, Y. Tao, X. H. Bu, *Cryst. Growth Des.* **2009**, *9*, 2280–2286.
[15] a) Y. P. Cai, Q. Y. Yu, Z. Y. Zhou, Z. J. Hu, H. C. Fang, N. Wang, Q. G. Zhan, L. Chen, C. Y. Su, *CrystEngComm* **2009**, *6*, 1006–1013; b) Y. C. Qiu, Z. H. Liu, J. X. Mou, H. Deng, M. Zeller, *CrystEngComm* **2010**, *12*, 277–290; c) H. Deng, Z. H. Liu, Y. C. Qiu, Y. H. Li, M. Zeller, *Inorg. Chem. Commun.* **2008**, *11*, 978–981; d) G. Mezei, J. W. Kampf, S. L. Pan, K. R. Poeppelmeier, B. Watkins, V. L. Pecoraro, *Chem. Commun.* **2007**, 1148–1150.
[16] a) A. L. Spek, *PLATON, A Multipurpose Crystallographic Tool*, Utrecht University, Utrecht, **2005**; b) A. L. Spek, *Acta Crystallogr., Sect. D* **2009**, *65*, 148–155.
[17] a) L. F. Ma, X. Q. Li, Q. L. Meng, L. Y. Wang, M. Du, H. W. Hou, *Cryst. Growth Des.* **2011**, *11*, 175–184; b) C. S. B. Gomes, D. Suresh, P. T. Gomes, L. F. Verios, M. T. Duarte, T. G. Nunes, M. C. Qliveira, *Dalton Trans.* **2010**, *39*, 736–748.
[18] X. W. Wang, J. Z. Chen, J. H. Liu, *Cryst. Growth Des.* **2007**, *7*, 1227–1229.
[19] a) J. Y. Zhang, A. L. Cheng, Q. Sun, Q. Yue, E. Q. Gao, *Cryst. Growth Des.* **2010**, *10*, 2908–2915; b) X. Q. Liang, J. T. Jia, T. Wu, D. P. Li, L. Liu, Tsolmon, G. S. Zhu, *CrystEngComm* **2010**, *11*, 3499–3501; c) M. F. Wu, F. K. Zheng, A. Q. Wu, Y. Li, M. S. Wang, W. W. Zhou, F. Chen, G. C. Guo, J. S. Huang, *CrystEngComm* **2010**, *12*, 260–269.
[20] a) G. M. Sheldrick, *APEX II software, Version 3.1.2*, Bruker AXS Inc, Madison, Wisconsin, **2004**; b) G. M. Sheldrick, *SHELXL-97*, *Program for X-ray Crystal Structure Refinement*, University of Göttingen, Göttingen, **1997**; c) G. M. Sheldrick, *Acta Crystallogr., Sect. A* **2008**, *64*, 112–122.

Received: March 2, 2011
Published Online: July 6, 2011

